Author(s): Mustonen, Otto & Vasala, Sami & Chou, Ta-Lei & Chen, Jin-Ming & Karppinen, Maarit

Title: Competition between ferromagnetism and antiferromagnetism in the rutile Cr1-xVxO2 system

Year: 2016

Version: Final published version

Please cite the original version:

Mustonen, Otto & Vasala, Sami & Chou, Ta-Lei & Chen, Jin-Ming & Karppinen, Maarit. 2016. Competition between ferromagnetism and antiferromagnetism in the rutile Cr1-xVxO2 system. Physical Review B. Volume 93, Issue 1. 10. DOI: 10.1103/physrevb.93.014405.

Competition between ferromagnetism and antiferromagnetism in the rutile $Cr_{1-x}V_xO_2$ system

Otto Mustonen,[1] Sami Vasala,[1,2] Ta-Lei Chou,[1] Jin-Ming Chen,[3] and Maarit Karppinen[1,*]
[1]*Department of Chemistry, Aalto University, FI-00076 AALTO, Finland*
[2]*Laboratory of Photonics and Interfaces, Institute of Chemical Sciences and Engineering, École Polytechnique Fédérale de Lausanne (EPFL), 1015 Lausanne, Switzerland*
[3]*National Synchrotron Radiation Research Center, Hsinchu 30076, Taiwan*
(Received 5 October 2015; revised manuscript received 15 November 2015; published 6 January 2016)

We present a comprehensive computational and experimental examination of the $Cr_{1-x}V_xO_2$ ($0 \leqslant x \leqslant 0.5$) system. The entire series crystallizes in the rutile structure, but the compounds exhibit significantly different magnetic properties depending on x. Lattice parameter a increases linearly with x, but the c parameter is slightly reduced due to vanadium-vanadium bonding. The V-for-Cr substitution creates Cr^{3+}-V^{5+} pairs; this leads to competition between ferromagnetic (Cr^{4+}-Cr^{4+}) and antiferromagnetic (Cr^{3+}-Cr^{3+}) interactions such that the materials change from ferromagnetic to antiferromagnetic with increasing x. Weak ferromagnetic interactions arising from Cr^{4+} are observed even in the seemingly antiferromagnetic phases with the exception of $x = 0.5$, which contains only Cr^{3+}. Density functional theory calculations are performed, but they incorrectly predict the $x = 0.5$ phase to be a half-metal. This is caused by an incorrect prediction of the oxidation states of chromium and vanadium.

DOI: 10.1103/PhysRevB.93.014405

I. INTRODUCTION

Half-metallic ferromagnets are materials in which a metallic band crosses the Fermi level for one spin channel while a band gap exists in the other spin channel [1,2]. This should yield a 100% spin polarization of charge carriers at very low temperatures. Half-metallic ferromagnets are promising materials for spintronics applications for magnetic tunneling junctions or as sources of spin-polarized electrons [2]. Half-metallic materials include chromium dioxide (CrO_2) [3,4], Heusler alloys, such as NiMnSb [5], the perovskite (La, Sr)MnO_3 [6], double perovskites, such as Sr_2FeMoO_6 [7], and the recently discovered quadruple perovskite $CaCu_3Fe_2Re_2O_{12}$ [8].

Among the known half-metals, CrO_2 has the highest reported spin polarization of nearly 100% at 1.8 K [4] and a relatively high Curie temperature of ~395 K [9]. It is a metastable oxide of Cr^{4+} [9] and was first predicted to be a half-metal by density functional theory (DFT) calculations [3]. Half-metallicity of CrO_2 has been experimentally confirmed by superconducting point-contact measurements [4], spectroscopic methods [10], and from intergrain tunneling magnetoresistance [11]. Chromium dioxide is a self-doped double exchange ferromagnet with one of the two t_{2g} d electrons localized and one itinerant [12]. It crystallizes in the tetragonal rutile structure (the inset in Fig. 1, space group $P4_2/mnm$), which is common for transition-metal dioxides [13].

Vanadium dioxide, in contrast, is known for a metal-insulator transition (MIT) at 340 K from a high-temperature rutile phase to a monoclinic insulating M_1 phase [14]. The rutile phase is paramagnetic whereas the M_1 phase is diamagnetic. The magnetic ground state of the rutile-structured VO_2, which is not experimentally obtainable due to the MIT, is still under debate. Many DFT methods predict a half-metallic ferromagnetic ground state for rutile VO_2 similar to that of CrO_2 [15,16]. Room-temperature ferromagnetism was recently discovered in thin films of rutile-structured VO_2 partially substituted with chromium [17]. In bulk, these $V_xCr_{1-x}O_2$ ($0.8 \leqslant x \leqslant 0.9$) compounds exhibit a structural transition from a monoclinic $P2/m$ M_4 phase to a semiconducting rutile high-temperature phase [18]. However, thin films grown on a (001) Al_2O_3 substrate are stable in the rutile phase down to 100 K, and the semiconductor-insulator transition is suppressed [17,19]. DFT calculations by Williams *et al.* [15] predicted these stabilized rutile $V_xCr_{1-x}O_2$ compounds to be not only ferromagnetic, but also half-metallic. Nevertheless, a later experimental study revealed $V_{0.82}Cr_{0.18}O_2$ to be a ferromagnetic insulator [19]. Finally, DFT calculations also predict the Cr-rich $Cr_{0.75}V_{0.25}O_2$ to remain half-metallic with a ferromagnetic coupling of Cr^{4+} (d^2) and V^{4+} (d^1) [20].

These theoretical predictions raise the question of whether new half-metals with the rutile structure exist in the CrO_2-VO_2 system. For this reason, we have investigated a relatively unknown rutile phase in this system, namely, the tetragonal high-pressure phase of $CrVO_4$. The ambient pressure form of $CrVO_4$ is orthorhombic with an octahedral coordination of Cr^{3+} and a tetrahedral coordination of V^{5+} [21]. Under high-pressure high-temperature conditions [22] or mechanochemical synthesis [23,24] the material is reported to adopt the rutile structure increasing the coordination number of vanadium to six. However, the exact crystal structure has not been solved. Moreover, the physical properties of this rutile phase have not been reported.

In this paper we report on the synthesis, crystal structure, magnetism, oxidation state, and electronic structure of $Cr_{1-x}V_xO_2$ $0 \leqslant x \leqslant 0.5$ phases. To accomplish this, we utilize high-pressure synthesis, x-ray diffraction and Rietveld refinement, dc magnetization measurements, synchrotron x-ray absorption spectroscopy, and DFT calculations. We find competitive ferromagnetic (FM) and antiferromagnetic (AFM) interactions arising from an unexpected combination of oxidation states.

*Corresponding author: maarit.karppinen@aalto.fi

II. EXPERIMENTAL DETAILS

A series of $Cr_{1-x}V_xO_2$ samples with $x = 0$, 0.1, 0.2, 0.3, 0.4, and 0.5 were prepared by high-pressure synthesis. Stoichiometric amounts of Cr_2O_3 (99.97%, Sigma-Aldrich), CrO_3 (99.99%, Sigma-Aldrich), and V_2O_5 (99.99%, Sigma-Aldrich) were thoroughly ground in an agate mortar. The resulting precursor mixtures were enclosed in gold capsules. CrO_3 is a highly hygroscopic compound; hence weighing and grinding of the powders and sealing the gold capsules were performed in a glove box under an argon atmosphere for all samples except $x = 0.5$, which does not require CrO_3 as a precursor. Synthesis was carried out in a cubic-anvil high-pressure apparatus (Riken-Seiki) at ∼4 GPa and 800 °C for 1 h. The sample was quenched to room temperature before gradually releasing the pressure.

Phase purity and crystal structure of the samples were investigated with x-ray powder diffraction (XRD; Pananalytical X'Pert Pro MPD, Cu $K\alpha_1$ radiation 1.540 60 Å). The diffraction patterns were collected in a continuous mode in the 2θ range of 10°–120° with a step size of 0.013°. Rietveld refinement was performed using the program FULLPROF [25]. The diffraction patterns were indexed with DICVOL [26].

Magnetic properties of the samples were investigated using a Quantum Design MPMS XL superconducting quantum interference device (SQUID) magnetometer; dc magnetic susceptibility was measured from 5 to 400 K using a measuring field of 1000 Oe. Both zero-field-cooled and field-cooled curves were measured. Isothermal magnetization curves were measured at 5 K from −50 to 50 kOe.

The oxidation states of samples were investigated by x-ray absorption spectroscopy (XAS). The XAS spectra were collected at the BL20A high-energy spherical grating monochromator beamline at the National Synchrotron Radiation Research Center in Taiwan. Vanadium and chromium $L_{2,3}$ edges corresponding to transitions from V or Cr $2p_{1/2}$ and $2p_{3/2}$ states to $3d$ states were measured. Additionally, an oxygen K edge corresponding to transitions from O $1s$ states to $2p$ states was measured. The spectra were collected in both total electron yield (TEY) and fluorescence yield (FY) modes except for Cr $L_{2,3}$, which was only collected in the TEY mode. The samples were mounted on a holder inside an ultrahigh vacuum chamber ($\sim 10^{-10}$ Torr), and the incidental photon flux I_0 was monitored with a gold-coated mesh located at the entrance to the vacuum chamber. The absorption features of single-crystal references located in the light path were recorded simultaneously and used for photon energy calibration.

III. COMPUTATIONAL DETAILS

Density functional theory calculations were performed in order to investigate the electronic structure of rutile $CrVO_4$ ($Cr_{0.5}V_{0.5}O_2$). The all-electron full-potential linearized plane-wave plus local orbitals ELK code [27] was used with the generalized gradient approximation (GGA) exchange and correlation functionals by Perdew, Burke, and Ernzerhof [28] (DFT-PBE). Electron correlation effects are significant in $3d$ transition-metal oxides due to the localized nature of the d electrons. DFT often has major difficulties predicting the physical properties of such strongly correlated systems, but multiple approaches exist to improve the agreement with experiment. Here we take electron correlation effects of Cr and V d electrons into account within the DFT-PBE + U framework with U and J as parameters [29–31]. The choice of the value for the Coulomb term U is often difficult. Previous DFT studies on CrO_2 have largely used the parameters $U = 3$ and $J = 0.9$ eV [12,20,32,33]. Recently experimental evidence in the form of hard x-ray photoemission spectroscopy was presented supporting a value of $U = 3.2$ eV [34].

In order to understand the effects of vanadium substitution on CrO_2, we started by comparing a hypothetical FM state of $Cr_{0.5}V_{0.5}O_2$ to the half-metallic ground state of CrO_2. Moreover, this also provides an easy comparison to previous DFT studies on $Cr_{0.75}V_{0.25}O_2$ [20] and $V_{0.75}Cr_{0.25}O_2$ [15], which both predicted a half-metallic FM ground state. The initial calculations were performed in simple six-atom rutile cells with the experimental crystal structure (Ref. [35] for CrO_2 and present data for $Cr_{0.5}V_{0.5}O_2$). A Monkhorst-Pack [36] k-point grid of $10 \times 10 \times 16$ was used for both compounds. An on-site Coulomb term of $U = 3$ eV and an exchange term of $J = 0.9$ eV were used for d electrons of chromium and vanadium.

An AFM state for $Cr_{0.5}V_{0.5}O_2$ in accordance with the experimental results was also examined. For this purpose, a 12-atom $2 \times 1 \times 1$ supercell was created. A simple AFM state where the corner and middle atoms of the rutile cell have opposite spins was considered and compared to the corresponding FM state. This type of approach with $U = 3$ eV was found to be sufficiently accurate for describing the electronic structure of antiferromagnetic rutile-type β-MnO_2 in which the experimental magnetic structure is a spin spiral [37]. A k-point grid of $5 \times 10 \times 16$ was used for the 12-atom supercell calculations, and the Coulomb U term was varied in the range of 2–6 eV. All calculations were performed with a plane-wave cutoff of $|G + k|_{\max} = 8/R_{\mathrm{MT}}$ a.u.$^{-1}$, where R_{MT} was the radius of the smallest muffin tin (oxygen, 1.5 a.u.).

IV. RESULTS

A. Experimental results

All the $Cr_{1-x}V_xO_2$ samples were black powders, and they did not sinter into pellets during the high-pressure high-temperature synthesis. The black color indicates that the materials might be metallic or narrow band-gap semiconductors. X-ray diffraction patterns for the $Cr_{1-x}V_xO_2$ samples are presented in Fig. 1. We were able to index every reflection in the diffraction patterns of all samples in the $P4_2/mnm$ space group of the rutile structure. Thus, all samples appear to be single phase while retaining the basic rutile structure. Crystallinity of the $x = 0.4$ phase was consistently slightly worse than for the others as seen from the broadened peaks and high peak asymmetry especially on the (110) reflection, but no additional peaks arising from impurities were found. Nevertheless, this suggests an immiscibility gap might exist between $x = 0.4$ and 0.5.

Gathering of high-quality XRD data for Rietveld refinement was made more challenging by two factors. First, the available sample size from the high-pressure synthesis was only around 40 mg. More importantly, CrO_2 tends to grow as needlelike crystals [9]. This leads to a significant preferred orientation in the XRD patterns. The orientation was fitted using the

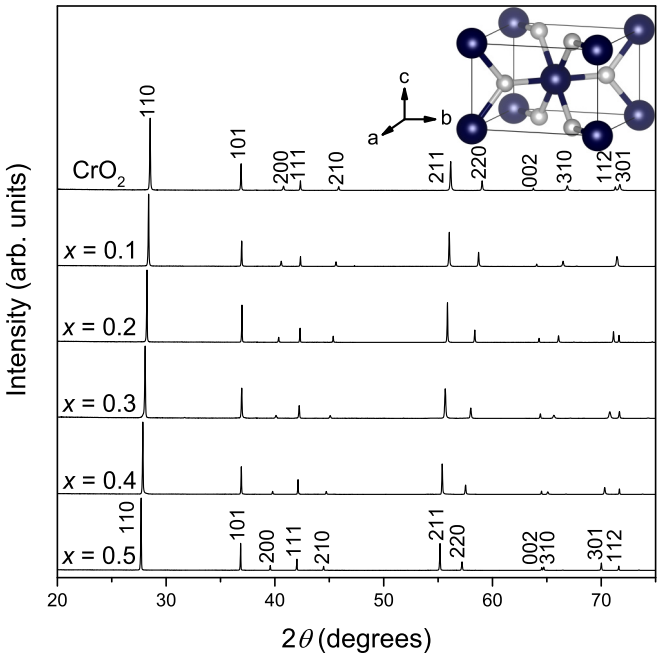

FIG. 1. X-ray diffraction patterns of $Cr_{1-x}V_xO_2$. Reflections corresponding to the space group $P4_2/mnm$ are indexed. The inset: The tetragonal rutile structure of CrO_2. The dark spheres represent chromium, and the gray spheres represent oxygen.

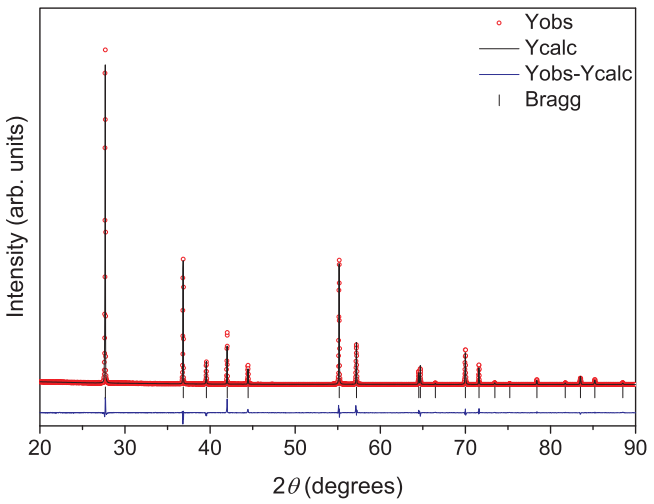

FIG. 2. Rietveld refinement result of $Cr_{0.5}V_{0.5}O_2$ ($x = 0.5$). The circles represents observed intensity, the black line is calculated intensity from the model, and the lower line is the difference curve. Bragg positions are indicated with vertical bars.

modified March function [38]. Refined $G1$ parameters were invariably larger than unity for all samples, confirming the needlelike shape of crystallites. In addition to orientation effects, needlelike crystallites also cause anisotropic size broadening. This broadening was fitted using a general phenomenological model described in Ref. [39]. Instrumental broadening was determined by measuring a LaB_6 standard (NIST SRM 660b) and assuming its crystallite size to be infinite. Refined crystallite sizes were in the microcrystalline range for all samples. Anisotropic size broadening was found to be significant with the c axis as the long axis as expected.

The crystal structure details of all samples were refined using the Rietveld method, see Fig. 2 as an example for the $x = 0.5$ sample. The results are gathered in Table I. All samples were refined in the rutile structure. The refinement results are good with the exception of the $x = 0.4$ sample, which is only satisfactory due to somewhat poor crystallinity.

In the case of CrO_2, our refined lattice parameters and oxygen positions are entirely in line with a neutron-diffraction study on bulk CrO_2 [35]. The effect of vanadium substitution on lattice parameters is shown in Fig. 3. The lattice parameter a increases linearly with x in accordance to Vegard's law. In contrast, the lattice parameter c slightly decreases as x increases in $Cr_{1-x}V_xO_2$. This decrease can be attributed to stronger metal-metal bonding, as the M-M bond distance in rutiles is equal to c [13]. The deviation from linearity for the c parameter might be due to subtle changes in the electronic structure similar to what has been observed in $V_{1-x}Mo_xO_2$ [40]. The rutile structure is fully defined by its atoms, the lattice parameters a and c, and the position of oxygen u (u, u, 0). From Table I, in the $Cr_{1-x}V_xO_2$ system the relative position of oxygen stays constant within experimental error with a slight deviation for the $x = 0.5$ sample. In the rutile structure the MO_6 octahedron has four equal equatorial M-O bonds and two equal apical M-O bonds [13]. The MO_6 octahedron in CrO_2 is equatorially elongated, that is to say it has four long equatorial M-O bonds and two short apical M-O bonds. The MO_6 octahedron in all vanadium-substituted $Cr_{1-x}V_xO_2$ samples is apically elongated, similar to rutile VO_2.

TABLE I. Rietveld refinement results for $Cr_{1-x}V_xO_2$. Space group $P4_2/mnm$. Cr and V reside on the $2a$ site at (0,0,0), and O resides on the $4f$ site at (u, u, 0).

	CrO_2	$Cr_{0.9}V_{0.1}O_2$	$Cr_{0.8}V_{0.2}O_2$	$Cr_{0.7}V_{0.3}O_2$	$Cr_{0.6}V_{0.4}O_2$	$Cr_{0.5}V_{0.5}O_2$
a (Å)	4.420 75(2)	4.443 84(1)	4.468 56(1)	4.494 27(2)	4.528 99(2)	4.551 41(1)
c (Å)	2.916 83(1)	2.904 85(1)	2.896 40(1)	2.891 30(1)	2.887 66(1)	2.886 26(1)
c/a	0.6598	0.6537	0.6482	0.6433	0.6376	0.6341
V(Å^3)	57.0037	57.3643	57.8352	58.3997	59.2310	59.7898
O u	0.3028(4)	0.3024(5)	0.3028(4)	0.3025(4)	3.030(5)	0.3050(4)
R_p (%)	20.1	19.8	20.7	20.1	22.1	16.2
R_{wp} (%)	20.4	20.9	21.0	20.6	24.2	17.5
χ^2	5.88	7.57	7.10	6.06	13.0	6.07

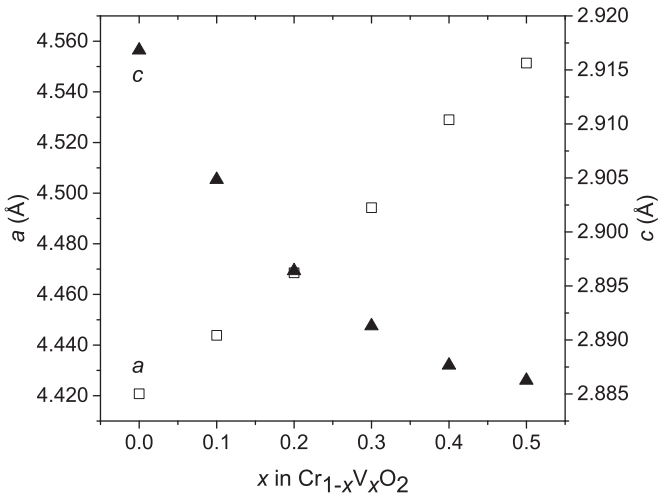

FIG. 3. Lattice parameters a and c as a function of x in $Cr_{1-x}V_xO_2$.

No additional reflections arising from cation ordering were observed in the XRD patterns (Fig. 1). The possibility of cation ordering was, nevertheless, considered. In the main known dirutile structures $CoReO_4$ and $MgUO_4$ the cations order in the ab plane [41]. These structures are orthorhombic, however, which rules out this type of ordering for our samples. Cation ordering in the c direction, which retains the tetragonal structure, is only known to occur in the high-pressure form of $GaAsO_4$ [42,43]. We simulated XRD patterns with the $GaAsO_4$-type ordering using the program FULLPROF [25]. The main simulated superlattice reflections were found to be less than 0.2% of intensity of the main peak. Since the expected additional reflections are so weak, we cannot entirely rule out the possibility of cation ordering.

Magnetic properties of the $Cr_{1-x}V_xO_2$ compounds are gathered in Table II. The types of magnetic ordering in the samples are visualized in Fig. 4, which represents the temperature-dependent magnetization curves. Curie temperatures for FM or ferrimagnetic (FiM) samples were determined from the inflection points in the $M(T)$ curves, see the inset in Fig. 4(a). The parent CrO_2 is FM with a sharp increase in susceptibility in the vicinity of the Curie temperature, see Fig. 4(a). Below T_C (396 K) on cooling, the susceptibility of CrO_2 rises to a near-constant value. The effect of vanadium substitution is clear in the $x = 0.1$ sample. Just 10% vanadium substitution lowers the T_C by almost 140 K down to 260 K,

TABLE II. Magnetic properties of the $Cr_{1-x}V_xO_2$ series. Coercivity was measured at 5 K. Effective paramagnetic moment and Weiss temperature were obtained from fits to Curie-Weiss law.

	T_C(K)	T_N(K)	Coercivity (Oe)	$\mu_{\text{eff}}(\mu_B)$	Θ (K)
CrO_2	396		~50	2.88[a]	360[a]
$Cr_{0.9}V_{0.1}O_2$	260		~50	~3	~300
$Cr_{0.8}V_{0.2}O_2$	114		1200	2.85	244
$Cr_{0.7}V_{0.3}O_2$		18	1500	2.72	148
$Cr_{0.6}V_{0.4}O_2$		16	1250	2.49	34
$Cr_{0.5}V_{0.5}O_2$		14	500	2.43	− 87

[a]Reference [9].

although the sample still appears to be FM. The $x = 0.2$ sample is no longer FM but has a broad maximum in susceptibility at $T_{\max} = 54$ K. The $M(T)$ curve is consistent with type P FiM ordering [44] with a T_C of 114 K, although the true ground state is not known. Samples with $x = 0.3$, 0.4, and 0.5 all appear to be AFM as can be seen from Figs. 4(b) and 4(c). Magnetic susceptibility decreases by an order of magnitude from panel (a) to panel (b) and by another order of magnitude from panel (b) to panel (c). The Néel temperatures were determined by finding the maximum in the corresponding $\partial\chi_{\text{mol}}T/\partial T$ curve, which is more accurate than using the maximum in susceptibility [45]. Néel temperatures decrease with increasing x from 18 K for $x = 0.3$ to 14 K for $x = 0.5$ (Table II). Reciprocal magnetic susceptibility is shown in panel (d).

Saturation magnetization M_s of a ferromagnet at 0 K is related to the spin of the cation by the formula $M_s = ngS\mu_B$ in which n is the number of cations per formula unit, g is the Landé g factor, S is the total spin angular momentum, and μ_B is the Bohr magneton. For CrO_2 (Cr^{4+} d^2, $S = 1$) this yields an expected saturation magnetization of $2\mu_B$ per Cr atom. Field-dependent magnetization curves measured at 5 K are presented in Fig. 5. Magnetization of CrO_2 saturates at fairly low fields of ~6 kOe to 1.89 μ_B per Cr atom. This is close to the expected theoretical value and significantly higher than in commercial CrO_2 powders [46]. The $x = 0.1$ sample behaves in a similar fashion and quickly saturates to 1.78 μ_B per cation as the field increases. Both $x = 0$ (CrO_2) and $x = 0.1$ samples have coercivities lower than 50 Oe. Magnetization of the $x = 0.2$ sample reaches 1.13 μ_B per cation at 50 kOe but does not saturate. It has a clear hysteresis loop with a coercivity of 1200 Oe. These factors support our classification of the sample $x = 0.2$ as FiM. Surprisingly, the seemingly antiferromagnetic $x = 0.3$ sample also displays some hysteresis behavior (the inset in Fig. 5), but maximum magnetization is only 0.34 μ_B per cation. Magnetization curves of $x = 0.4$ and $x = 0.5$ are nearly straight lines as expected from antiferromagnetic materials, and the magnetization only reaches 0.07 and 0.09 μ_B per cation at 50 kOe. The existence of some coercivity might indicate frustration in these samples.

The Curie-Weiss law describes the behavior of many magnetic materials in the paramagnetic region significantly above their Curie/Néel temperatures: $\chi_{\text{mol}} = C/(T-\Theta)$, where χ_{mol} is the molar magnetic susceptibility, C is the Curie constant, T is the absolute temperature, and Θ is the Weiss temperature. Moreover, the effective paramagnetic moment μ_{eff} can be obtained from C *via* $\mu_{\text{eff}} = (3k_BC/N_A)^{1/2}$, where k_B is the Boltzmann constant and N_A is the Avogadro constant. The magnetic properties of our $Cr_{1-x}V_xO_2$ samples are summarized in Table II. Effective paramagnetic moments and the Weiss temperatures were determined by plotting χ_{mol}^{-1} as a function of temperature and fitting a linear function to the high-temperature paramagnetic region, see Fig. 4(d). We were only able to measure magnetization up to 400 K, and a reliable fit to the Curie-Weiss law requires data far above the magnetic transition temperature of the material. For this reason, we could not obtain a fit for CrO_2 ($T_C = 396$ K) and our fit for $x = 0.1$ ($T_C \sim 260$ K) is only approximate. From literature it is known that the effective paramagnetic moment of CrO_2 is 2.88 μ_B [9], close to the expected spin-only value of 2.83 μ_B. In the $Cr_{1-x}V_xO_2$ system, the average number

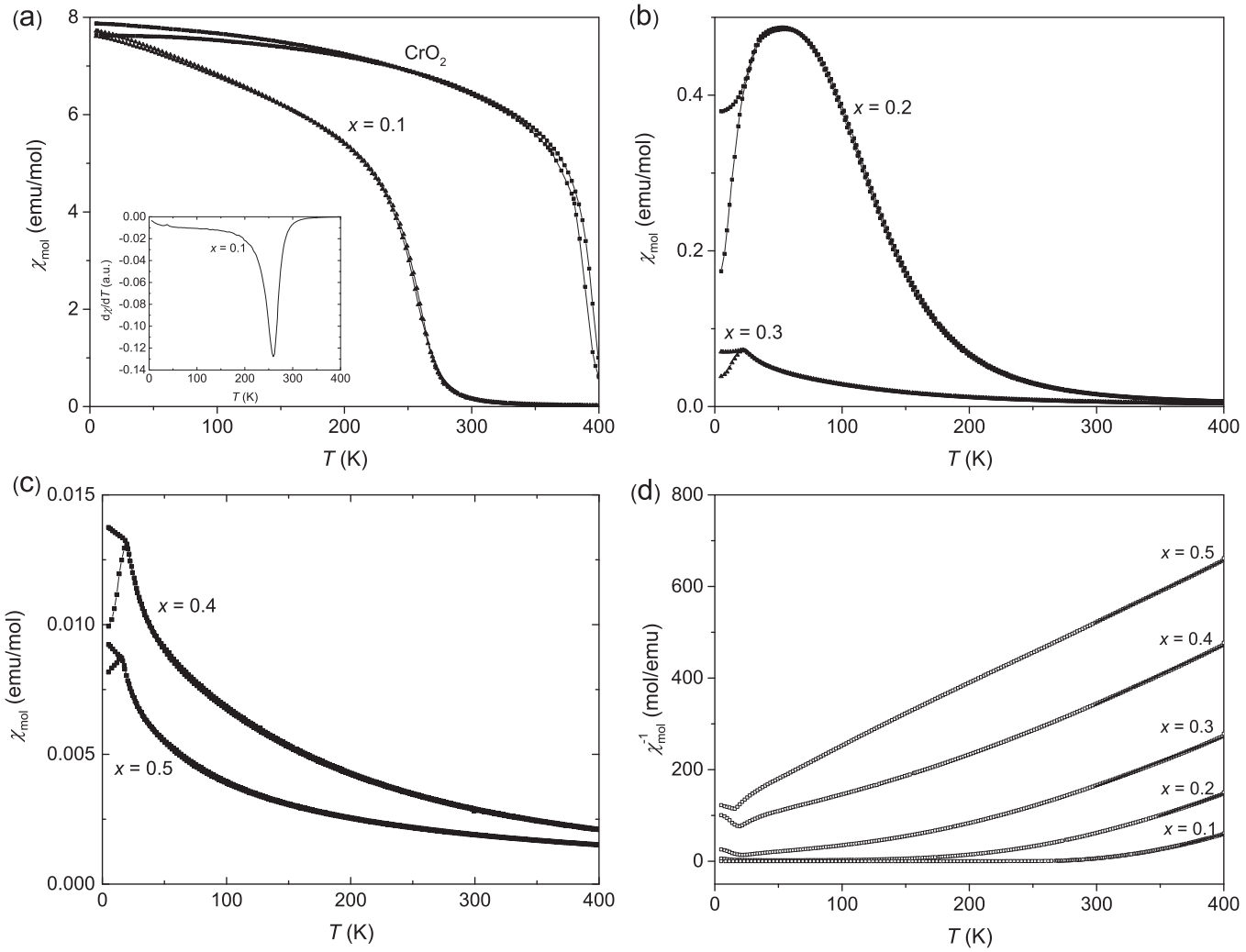

FIG. 4. Temperature-dependent magnetic susceptibility of $Cr_{1-x}V_xO_2$ samples measured at a field of 1000 Oe. (a) CrO_2 and $x = 0.1$ (the inset: derivate of magnetic susceptibility for $x = 0.1$), (b) $x = 0.2$ and $x = 0.3$, and (c) $x = 0.4$ and $x = 0.5$. (d) Reciprocal magnetic susceptibility as a function of temperature. The solid lines represent fits to Curie-Weiss law.

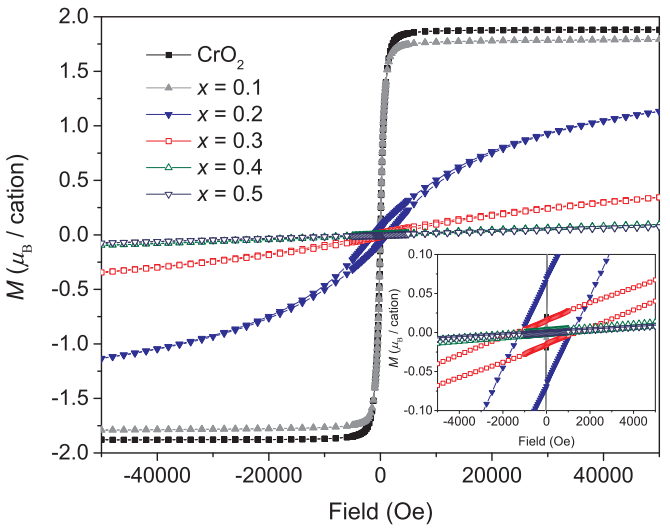

FIG. 5. Magnetization as a function of the external magnetic field of $Cr_{1-x}V_xO_2$ samples at 5 K. The inset: low-field magnetization. The symbols in the inset are the same as the symbols in the main figure.

of d electrons per cation decreases with increasing x, which is seen in the decrease in μ_{eff} down to 2.43 μ_B for $x = 0.5$. The Weiss temperatures of the samples are surprisingly high. Only $Cr_{0.5}V_{0.5}O_2$ has a negative Weiss temperature expected for antiferromagnetic materials. The positive Weiss constants might be an indication of lingering ferromagnetic interactions, such as weak ferromagnetism in $x = 0.3$ and 0.4.

Electronic structure and cation oxidation states in the $Cr_{1-x}V_xO_2$ samples were investigated by x-ray absorption spectroscopy. The spectra were collected in TEY and FY modes. The TEY signal comes from the electronic drain current, which has a relatively short escape length (∼100 Å) and is thereby surface sensitive. By contrast, FY gives information from the bulk (∼2000 Å) [47], but it unfortunately suffers from self-absorption for a number of main group and transition metals resulting in twisted spectra. For this reason, we will concentrate on the TEY spectra in the following discussion. The average crystallite size in the samples was several microns based on the line broadening analysis of XRD patterns.

Using surface techniques can be problematic for CrO_2 due to the formation of a thin native Cr_2O_3 layer on particle

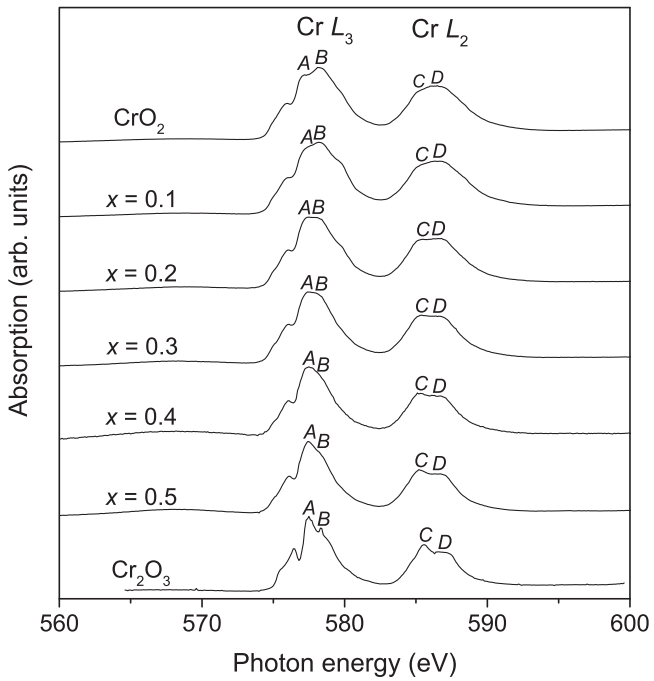

FIG. 6. X-ray absorption spectra of Cr $L_{2,3}$ edges in $Cr_{1-x}V_xO_2$ measured in the TEY mode. Spectral features highlighting the differences in Cr^{4+} (CrO_2) and Cr^{3+} (Cr_2O_3) are marked with letters.

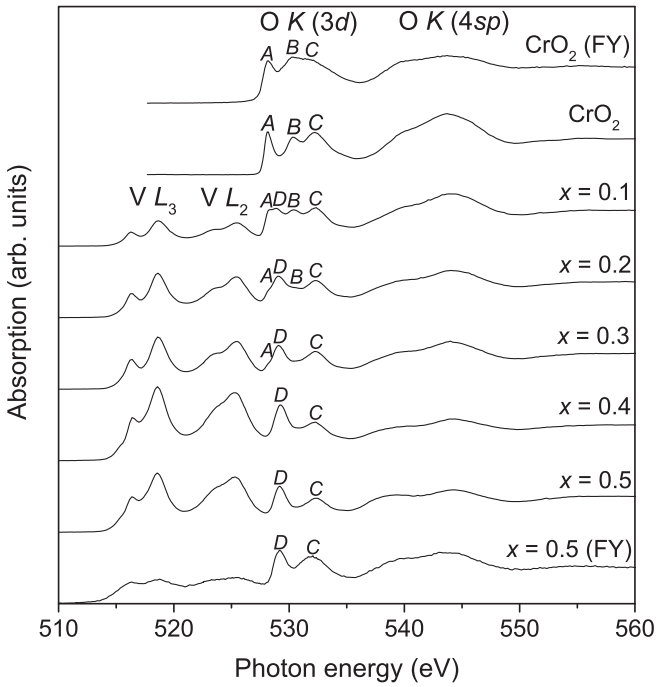

FIG. 7. X-ray absorption spectra of V $L_{2,3}$ and O K edges in $Cr_{1-x}V_xO_2$ measured in the TEY mode. Important spectral features are marked with letters. Spectra for $x = 0$ and 0.5 in the FY mode are included for comparison.

surfaces. In a previous XAS study [10] on CrO_2, the contribution of the surface Cr_2O_3 layer to the TEY Cr $L_{2,3}$ XAS spectra of CrO_2 was found to be negligible. Likewise, our recorded CrO_2 Cr $L_{2,3}$ spectrum (Fig. 6) in the TEY mode matches literature [10,48] and is clearly different from the Cr_2O_3 reference spectrum, showing that the native oxide layer does not contribute to XAS spectra for CrO_2. The main differences between the CrO_2 and the Cr_2O_3 spectra are highlighted with the letters A, B, C, and D in Fig. 6. It is evident that the spectral features shift from CrO_2-like to Cr_2O_3-like as x in $Cr_{1-x}V_xO_2$ increases. In the Cr $L_{2,3}$ spectrum of the $x = 0.5$ sample the spectral weight distributions of the features A, B, C, and D are essentially identical to those of Cr_2O_3. Thus we conclude that the oxidation state of chromium in $Cr_{1-x}V_xO_2$ shifts from Cr^{4+} towards Cr^{3+} as x increases. This conclusion is further supported by the recorded O K edges, which also allow us to confidently broaden this conclusion to the bulk as explained further below.

The combined V $L_{2,3}$ and O K XAS edges measured in the TEY mode are presented in Fig. 7. Two peaks at 516 and 519 eV are seen in the V $L_{2,3}$ spectra, and their positions and shapes do not change as a function of x. This might suggest that the oxidation state of vanadium is the same in all vanadium-substituted samples. However, given that the $L_{2,3}$ edges of V^{4+} and V^{5+} are difficult to differentiate [49], here we cannot accurately determine the valence state of vanadium. Moreover, the local environment of vanadium in $Cr_{1-x}V_xO_2$ is close to ideally octahedral whereas in V_2O_5, the XAS standard for V^{5+}, it is strongly distorted [50]. Nevertheless, we argue that vanadium is at an oxidation state of +V so that substituting chromium with vanadium creates Cr^{3+}-V^{5+} pairs, based on structural and magnetic factors. First, if vanadium is at +IV, the series becomes increasingly oxygen deficient with x ($Cr_{1-x}V_xO_{2-0.5x}$), whereas Cr^{3+}-V^{5+} pairs would make the series fully stoichiometric. Oxygen-deficient rutiles form Magnéli phases [51], which are structurally clearly different from the parent rutile phase. Since the $Cr_{1-x}V_xO_2$ series retains the rutile structure, the samples must be near stoichiometric and therefore contain Cr^{3+}-V^{5+} pairs. Second, refining oxygen occupancy from the XRD data does not suggest the existence of oxygen nonstoichiometry. Finally, the effective paramagnetic moment decreases with increasing x, which is consistent with Cr^{3+}-V^{5+} pairs, which result in a decrease in occupied d electrons, and not V^{4+} in which case the number of d electrons stays constant.

The oxygen K absorption edge, namely, the $1s$-$2p$ transition, is a powerful probe for transition-metal states hybridized with oxygen. The O K XAS spectra (Fig. 7) of CrO_2, recorded both in TEY and in FY modes, are similar to previous studies [48,52,53]. Our main interests are the features near 530 eV attributed to $3d$ states. In CrO_2, the octahedral crystal field splits the $3d$ orbitals into three t_{2g} and two e_g orbitals that are significantly hybridized with oxygen $2p$ orbitals. A slight distortion of the octahedron further splits the t_{2g} states into d_{xy}, d_{x+y}, and d_{x-y} states of which the first two are occupied in the up-spin channel (Cr^{4+} is d^2) [12,53]. We have highlighted the most important spectral features in Fig. 7 with the letters A (528 eV), B (530 eV), C (532 eV), and D (529 eV). Here, A is attributed to a transition to the single empty up-spin t_{2g} orbital of chromium (d_{x-y},), whereas the features B and C can be attributed to a combination of unoccupied up-spin e_g and down-spin t_{2g} and e_g states [52,53]. When some of the chromium is substituted with vanadium, we see the A peak lose intensity and finally disappear at $x = 0.4$. We attribute this to the gradual filling of the single unoccupied up-spin

t_{2g} orbital as chromium is reduced to Cr^{3+}. A new peak D is observed starting at $x = 0.1$. It is likely to arise mainly from V^{5+} t_{2g} states [50]. In the $x = 0.5$ sample, peak B likely mainly consists of V^{5+} e_g states [50] and Cr^{3+} t_{2g} and e_g states [54]. We like to emphasize that the O K edges were also measured in the bulk sensitive FY mode. These spectra have more noise, but all the central features of the TEY spectra are reproduced. The most important of these is the gradual disappearance of the A peak with increasing x, which is linked to the reduction of Cr^{4+} to Cr^{3+}. In Fig. 7 the FY O K spectra of the end members $x = 0$ and 0.5 are presented as examples. Since the TEY and FY spectra are nearly identical, the hybridization of chromium $3d$ states with oxygen and their occupancy must also be identical both near the surface (TEY) and in the bulk (FY). Thus, we can conclude that the reduction of chromium from Cr^{4+} towards Cr^{3+} is not limited only to the surface, but also occurs in the bulk.

B. Computational results

Electronic structures of CrO_2 and $Cr_{0.5}V_{0.5}O_2$ were studied by DFT calculations. We began by comparing the electronic structures of CrO_2 and a hypothetical FM state of $Cr_{0.5}V_{0.5}O_2$ ($x = 0.5$) to understand the effects of vanadium substitution. Both DFT-PBE ($U = 0$) and DFT-PBE + U calculations were performed for CrO_2 and $Cr_{0.5}V_{0.5}O_2$ ($x = 0.5$) starting from a FM six-atom cell. The $U = 0$ and $U = 3$ eV calculations gave similar results in both cases. The density of states of CrO_2 calculated with $U = 3$ eV is shown in Fig. 8(a). Our results for CrO_2 are similar to those reported in literature [12,20,32,33] showing that CrO_2 is a half-metallic ferromagnet in which the Fermi level lies near a local minimum in the up-spin channel and in a gap in the down-spin channel. The up-spin states near E_F consist of the two occupied and one unoccupied Cr t_{2g} states. The down-spin gap, on the other hand, forms between occupied O $2p$ states and unoccupied Cr t_{2g} states.

The theoretical FM state of $Cr_{0.5}V_{0.5}O_2$ [Fig. 8(b)] is in many ways similar to CrO_2. It, too, is a half-metallic ferromagnet. The total moment for the six-atom cell is $3\,\mu_B$ with a moment of $2.29\,\mu_B$ on chromium and $0.71\,\mu_B$ on vanadium, indicating that both vanadium and chromium are at an oxidation state of +IV and couple ferromagnetically. This result is similar to a previous DFT study [20] on $Cr_{0.75}V_{0.25}O_2$. Nevertheless, it is contrary to our experimental evidence (Figs. 6 and 7). As in CrO_2, E_F is located near a local minimum in the up-spin channel. Immediately below it is the single occupied vanadium t_{2g} state and then the two occupied chromium t_{2g} states down to −1 eV. States immediately above the Fermi level consist mostly of empty vanadium t_{2g} states. Interesting changes take place in the down-spin channel. Now the minority spin pseudogap exists between occupied oxygen $2p$ states at −1 eV and unoccupied vanadium t_{2g} states. The down-spin unoccupied chromium t_{2g} states are pushed up in energy to 3 eV and above.

Since experimentally $Cr_{0.5}V_{0.5}O_2$ is AFM, we investigated AFM states within the DFT-PBE + U framework using a 12-atom supercell and compared them to the corresponding FM states. The Coulomb U term was varied from 2 to 6 eV. The AFM solutions were metallic for DFT-PBE and U up to 4 eV, whereas a band gap opened for $U = 5$ eV. The magnetic moments on chromium were from 1.8 to $2\,\mu_B$ and on vanadium from 0.6 to $0.9\,\mu_B$, respectively. Thus, the antiferromagnetic solutions for $Cr_{0.5}V_{0.5}O_2$ predict chromium to be $Cr^{4+}(d^2, S = 1)$ and vanadium to be $V^{4+}(d^1, S = 1/2)$. This is in contrast to our experimental XAS data (Fig. 6), which clearly shows chromium to be Cr^{3+}. Moreover, the AFM states were not the ground states for the 12-atom supercell. The ground states were half-metallic FM states similar to the six-atom ground state presented in Fig. 8(b). The FM state was more stable than the AFM state by 47, 82, 93, 83, 47, and 22 meV/f.u. corresponding to $U = 0, 2-6$ eV, respectively. Thus, our DFT calculations predict $Cr_{0.5}V_{0.5}O_2$ to be a half-metallic ferromagnet, whereas experimentally we have shown it to be antiferromagnetic.

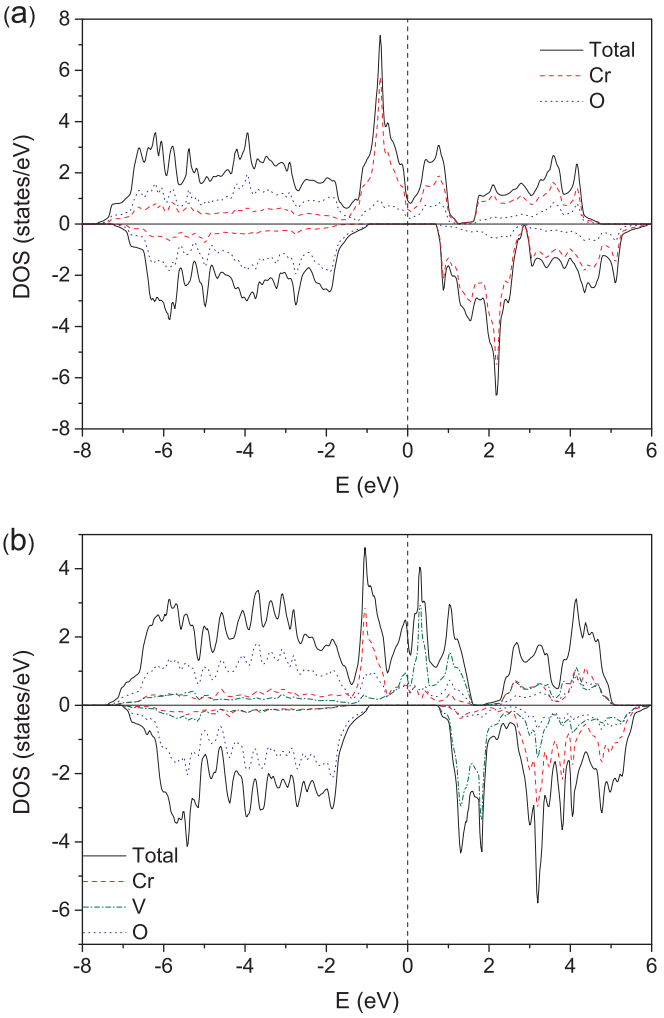

FIG. 8. Total and partial densities of states for ferromagnetic (a) CrO_2 and (b) $Cr_{0.5}V_{0.5}O_2$ ($x = 0.5$).

V. DISCUSSION

The oxidation states of chromium and vanadium are central to understanding the properties of $Cr_{1-x}V_xO_2$ compounds. Both chromium and vanadium form rutiles at the oxidation state +IV, namely, CrO_2 and the high-temperature phase of VO_2 [13,41]. There are two ways that chromium can be substituted with vanadium. One might assume that substitution

on the same site as is the case in $Cr_{1-x}V_xO_2$ would result in oxidation states of +IV for both cations, i.e., $Cr^{4+}{}_{1-x}V^{4+}{}_xO_2$. Indeed, this is the prediction from our DFT calculations and earlier DFT studies [15,20]. Moreover, V^{5+} is a relatively small cation that favors tetrahedral coordination over the octahedral coordination in rutiles. On the other hand, chromium might be reduced to Cr^{3+} and vanadium oxidized to V^{5+} forming Cr^{3+}-V^{5+} pairs, i.e., $Cr^{4+}{}_{1-2x}Cr^{3+}{}_xV^{5+}{}_xO_2$. Our x-ray absorption measurements on the Cr/V $L_{2,3}$ and O K edges (Figs. 6 and 7) reveal that this is the case. A similar result of the formation of Cr^{3+}-V^{5+} pairs was found in rutile-structured $V_{0.82}Cr_{0.18}O_2$ [19].

The d electron configurations of Cr^{4+}, Cr^{3+}, V^{4+}, and V^{5+} are d^2,d^3,d^1, and d^0, respectively. In the rutile structure, these cations are located in an octahedral crystal field. We can use these d electron configurations and the crystal structure to estimate the strength of exchange interactions in $Cr_{1-x}V_xO_2$. This can be performed using the semiempirical Goodenough-Kanamori rules [55,56] for superexchange in oxides. However, in the case of Cr^{4+}-Cr^{4+} interactions we can simply utilize existing more accurate determinations of exchange constants in CrO_2. Sims *et al.* [33] have calculated the most important exchange couplings in CrO_2 within the DFT-PBE framework. These were found to be $J_{100} = -12.2$ meV (from corner to corner on the ab plane, the inset in Fig. 1), $J_{001} = 27.5$ meV (from corner to corner along c), and $J_{111} = 20.7$ meV (from the corner to the middle cation). Thus, the exchange interactions are ferromagnetic overall (positive J), and CrO_2 is ferromagnetic.

In the Goodenough-Kanamori rules [55,56] the signs and relative strengths of the superexchange interactions between cations is considered based on the M-O-M angle and the number of d electrons. Superexchange interactions of Cr^{3+} tend to be AFM due to the half-filled t_{2g} orbitals. M-O-M angles corresponding to J_{100}, J_{001}, and J_{111} exchange couplings in rutiles are approximately 110°, 100°, and 130°, respectively. The overall 180° M-O-M superexchange interaction for d^3 is expected to be moderately to weakly antiferromagnetic [57]. The overall 90° M-O-M superexchange interactions for d^3 are also expected to be moderately to weakly antiferromagnetic [57]. Thus, we can predict all J_{100}, J_{001}, and J_{111} to be negative for Cr^{3+}-Cr^{3+} interactions. Cr^{3+}-V^{5+} (d^3-d^0) superexchange is expected to be very weak but ferromagnetic.

The magnetic properties of the $Cr_{1-x}V_xO_2$ compounds are the result of competing FM (Cr^{4+}-Cr^{4+}) and AFM (Cr^{3+}-Cr^{3+}) interactions. The Curie temperature of a ferromagnet is directly related to the sum of all exchange interactions in the mean-field Ising model of magnetism. Thus, the massive 140 K drop in T_C from CrO_2 to $x = 0.1$ [Fig. 4(a)] can be understood as the combination of a decrease in average FM couplings, i.e., less Cr^{4+}, and the increase in average AFM couplings, i.e., the Cr^{3+} formed. A further increase in AFM and a decrease in FM interactions lead to the $x = 0.2$ sample exhibiting FiM-type behavior. For $x = 0.4$ and 0.5 AFM interactions dominate resulting in temperature- and field-dependent behaviors typical of AFM ordering.

Magnetism in the $x = 0.3$ sample is more complex as its temperature-dependent behavior is similar to AFM materials, see Fig. 4(c), but the field-dependent magnetization exhibits a hysteresis loop (Fig. 5). The exact nature of the ground state of this sample remains unclear. Competing magnetic interactions, such as in these samples, can lead to magnetic frustration. Moreover, the $Cr_{1-x}V_xO_2$ samples have structural disorder due to the statistical distribution of Cr and V on the same lattice site. Frustration parameter f, defined as $f = |\Theta|/T_N$ (or T_C) gives a simple indication of the degree of magnetic frustration in a material [58]. For $x = 0.3$ we obtain $f = 8$, which is significantly higher than for the other samples. This indicates a moderate degree of frustration and is close to the limit of strong frustration ($f > 10$). The unusual magnetic properties of $x = 0.3$ might be a result of this magnetic frustration.

The $x = 0.2$ sample is FiM because the FM and AFM couplings are of similar magnitude. In the AFM $x = 0.3$ sample we can still see evidence of the FM Cr^{4+}-Cr^{4+} interactions since the compound exhibits a hysteresis loop at 5 K, see Fig. 5. Additionally, the Weiss constants of AFM $x = 0.3$ and 0.4 samples (Table II) are positive at 148 and 34 K due to the presence of FM interactions.

The formation of Cr^{3+} and V^{5+} pairs is also linked to our DFT calculations. DFT-PBE and DFT-PBE + U calculations resulted in the incorrect FM half-metallic ground state for $Cr_{0.5}V_{0.5}O_2$ as seen in Fig. 8(b). This is due to the fact that they failed to predict the correct oxidation states of chromium and vanadium. The DFT-PBE method is known to underestimate oxidation energies in transition metals [59]. It places an energy penalty on the reduced state due to the insufficient inclusion of electron correlation effects. This can be corrected to a degree within the DFT-PBE + U framework [59]. However, in our calculations increasing the on-site Coulomb term U did not result in Cr^{3+} and V^{5+}. The application of more sophisticated approaches to this problem, such as meta-GGA, hybrid functionals, or Green's-function-based methods are beyond the scope of this paper. Most half-metals contain more than one transition metal. Thus, incorrectly predicting the oxidation states of transition metals is a potential issue in the *ab initio* search for new half-metals.

VI. CONCLUSIONS

We have investigated magnetism in the $Cr_{1-x}V_xO_2$ system using experimental and computational methods. A series of compounds with $0 \leqslant x \leqslant 0.5$ were prepared by high-pressure synthesis. All samples crystallize in the tetragonal rutile structure (space group $P4_2/mnm$). Lattice parameter a increases with increasing x in accordance to Vegard's law. A small decrease in the lattice parameter c was observed and attributed to vanadium-vanadium bonding. The MO_6 octahedron is apically elongated for $x > 0$. No evidence of cation ordering was found.

X-ray absorption spectroscopy at the Cr/V $L_{2,3}$ edges and the O K edge revealed the vanadium substitution to result in the formation of pairs of Cr^{3+} and V^{5+} cations. Existence of both Cr^{4+} and Cr^{3+} in $Cr_{1-x}V_xO_2$ leads to competition between ferromagnetic (Cr^{4+}-Cr^{4+}, d^2-d^2) and antiferromagnetic (Cr^{3+}-Cr^{3+}, d^3-d^3) interactions. This effect is so significant that even a moderate substitution at $x = 0.1$ results in a 140-K drop in the Curie temperature. A further increase in x results in ferrimagnetism ($x = 0.2$) and finally antiferromagnetism ($x = 0.3$,0.4,0.5) based on susceptibility and magnetization data, but the true nature of the ground states

remains unclear. Existence of weak ferromagnetic interactions in the antiferromagnetic $x = 0.3$ and 0.4 samples is evidenced by the positive Weiss temperatures. Curiously, the $x = 0.3$ sample exhibits a hysteresis loop at 5 K, despite AFM-like temperature-dependent behavior, indicating that the ground state could be more complex.

Density functional theory calculations resulted in an incorrect half-metallic ground state for $x = 0.5$. This was attributed to a failure to predict the oxidation states of chromium and vanadium, a common problem with transition-metal oxides in DFT. This result highlights a potential difficulty in the search for new half-metals by DFT.

ACKNOWLEDGMENTS

The authors acknowledge CSC–IT Centre for Science, Finland, for providing computational resources. Dr. E.-L. Rautama is thanked for assistance with the Rietveld refinement. The program VESTA3 [60] was used to draw the inset in Fig. 1.

[1] R. A. de Groot, F. M. Mueller, P. G. van Engen, and K. H. J. Buschow, Phys. Rev. Lett. **50**, 2024 (1983).
[2] M. I. Katsnelson, V. Y. Irkhin, L. Chioncel, A. I. Lichtenstein, and R. A. de Groot, Rev. Mod. Phys. **80**, 315 (2008).
[3] K. Schwarz, J. Phys. F: Met. Phys. **16**, L211 (1986).
[4] R. J. Soulen, J. M. Byers, M. S. Osofsky, B. Nadgorny, T. Ambrose, S. F. Cheng, P. R. Broussard, C. T. Tanaka, J. Nowak, J. S. Moodera, A. Barry, and J. M. D. Coey, Science **282**, 85 (1998).
[5] C. T. Tanaka, J. Nowak, and J. S. Moodera, J. Appl. Phys. **86**, 6239 (1999).
[6] J.-H. Park, E. Vescovo, H.-J. Kim, C. Kwon, R. Ramesh, and T. Venkatesan, Nature (London) **392**, 794 (1998).
[7] K.-I. Kobayashi, T. Kimura, H. Sawada, K. Terakura, and Y. Tokura, Nature (London) **395**, 677 (1998).
[8] W. Chen, M. Mizumaki, H. Seki, M. S. Senn, T. Saito, D. Kan, J. P. Attfield, and Y. Shimakawa, Nat. Commun. **5**, 3909 (2014).
[9] B. L. Chamberland, Crit. Rev. Solid State Mater. Sci. **7**, 1 (1977).
[10] Y. S. Dedkov, A. S. Vinogradov, M. Fonin, C. König, D. V. Vyalikh, A. B. Preobrajenski, S. A. Krasnikov, E. Y. Kleimenov, M. A. Nesterov, U. Rüdiger, S. L. Molodtsov, and G. Güntherodt, Phys. Rev. B **72**, 060401 (2005).
[11] J. M. D. Coey, A. E. Berkowitz, L. Balcells, F. F. Putris, and A. Barry, Phys. Rev. Lett. **80**, 3815 (1998).
[12] M. A. Korotin, V. I. Anisimov, D. I. Khomskii, and G. A. Sawatzky, Phys. Rev. Lett. **80**, 4305 (1998).
[13] A. A. Bolzan, C. Fong, B. J. Kennedy, and C. J. Howard, Acta Crystallogr., Sect. B: Struct. Sci. **B53**, 373 (1997).
[14] Z. Yang, C. Ko, and S. Ramanathan, Annu. Rev. Mater. Res. **41**, 337 (2011).
[15] M. E. Williams, W. H. Butler, C. K. Mewes, H. Sims, M. Chshiev, and S. K. Sarker, J. Appl. Phys. **105**, 07E510 (2009).
[16] B. Xiao, J. Sun, A. Ruzsinszky, and J. P. Perdew, Phys. Rev. B **90**, 085134 (2014).
[17] K. G. West, J. Lu, L. He, D. Kirkwood, W. Chen, T. P. Adl, M. S. Osofsky, S. B. Qadri, R. Hull, and S. A. Wolf, J. Supercond. Novel Magn. **21**, 87 (2008).
[18] J. B. Goodenough and H. Y.-P. Hong, Phys. Rev. B **8**, 1323 (1973).
[19] L. F. J. Piper, A. DeMasi, S. W. Cho, A. R. H. Preston, J. Laverock, K. E. Smith, K. G. West, J. W. Lu, and S. A. Wolf, Phys. Rev. B **82**, 235103 (2010).
[20] M. E. Williams, H. Sims, D. Mazumdar, and W. H. Butler, Phys. Rev. B **86**, 235124 (2012).
[21] E. J. Baran, J. Mater. Sci. **33**, 2479 (1998).
[22] A. P. Young and C. M. Schwartz, Acta Crystallogr. **15**, 1305 (1962).
[23] T. Tojo, Q. Zhang, and F. Saito, J. Solid State Chem. **179**, 433 (2006).
[24] Q. Zhang, T. Tojo, W. Tongamp, and F. Saito, Powder Technol. **195**, 40 (2009).
[25] J. Rodríguez-Carvajal, Physica B **192**, 55 (1993).
[26] A. Boultif and D. Louër, J. Appl. Crystallogr. **37**, 724 (2004).
[27] http://elk.sourceforge.net.
[28] J. P. Perdew, K. Burke, and M. Ernzerhof, Phys. Rev. Lett. **77**, 3865 (1996).
[29] V. I. Anisimov, J. Zaanen, and O. K. Andersen, Phys. Rev. B **44**, 943 (1991).
[30] V. I. Anisimov, I. V. Solovyev, M. A. Korotin, M. T. Czyżyk, and G. A. Sawatzky, Phys. Rev. B **48**, 16929 (1993).
[31] A. I. Liechtenstein, V. I. Anisimov, and J. Zaanen, Phys. Rev. B **52**, R5467 (1995).
[32] L. Chioncel, H. Allmaier, E. Arrigoni, A. Yamasaki, M. Daghofer, M. I. Katsnelson, and A. I. Lichtenstein, Phys. Rev. B **75**, 140406 (2007).
[33] H. Sims, S. J. Oset, W. H. Butler, J. M. MacLaren, and M. Marsman, Phys. Rev. B **81**, 224436 (2010).
[34] M. Sperlich, C. König, G. Güntherodt, A. Sekiyama, G. Funabashi, M. Tsunekawa, S. Imada, A. Shigemoto, K. Okada, A. Higashiya, M. Yabashi, K. Tamasaku, T. Ishikawa, V. Renken, T. Allmers, M. Donath, and S. Suga, Phys. Rev. B **87**, 235138 (2013).
[35] J. K. Burdett, G. J. Miller, J. W. Richardson, and J. V. Smith, J. Am. Chem. Soc. **110**, 8064 (1988).
[36] H. J. Monkhorst and J. D. Pack, Phys. Rev. B **13**, 5188 (1976).
[37] C. Franchini, R. Podloucky, J. Paier, M. Marsman, and G. Kresse, Phys. Rev. B **75**, 195128 (2007).
[38] W. A. Dollase, J. Appl. Crystallogr. **19**, 267 (1986).
[39] J. Rodríquez-Carvajal and T. Roisnel, Mater. Sci. Forum **443-444**, 123 (2004).
[40] K. L. Holman, T. M. McQueen, A. J. Williams, T. Klimczuk, P. W. Stephens, H. W. Zandbergen, Q. Xu, F. Ronning, and R. J. Cava, Phys. Rev. B **79**, 245114 (2009).
[41] W. H. Baur, Crystallogr. Rev. **13**, 65 (2007).
[42] S. Matar, M. Lelogeais, D. Michau, and G. Demazeau, Mater. Lett. **10**, 45 (1990).
[43] W. Duan, R. M. Wentzcovitch, and J. R. Chelikowsky, Phys. Rev. B **60**, 3751 (1999).

[44] S. Chikazumi, *Physics of Ferromagnetism*, 2nd ed. (Clarendon, Oxford, 1997).
[45] E. E. Bragg and M. S. Seehra, Phys. Rev. B **7**, 4197 (1973).
[46] A. Bajpai and A. K. Nigam, Appl. Phys. Lett. **87**, 222502 (2005).
[47] L. Tröger, D. Arvanitis, H. Rabus, L. Wenzel, and K. Baberschke, Phys. Rev. B **41**, 7297 (1990).
[48] D. J. Huang, H.-T. Jeng, C. F. Chang, G. Y. Guo, J. Chen, W. P. Wu, S. C. Chung, S. G. Shyu, C. C. Wu, H.-J. Lin, and C. T. Chen, Phys. Rev. B **66**, 174440 (2002).
[49] R. Zimmermann, R. Claessen, F. Reinert, P. Steiner, and S. Hüfner, J. Phys.: Condens. Matter **10**, 5697 (1999).
[50] C. Hébert, M. Willinger, D. S. Su, P. Pongratz, P. Schattschneider, and R. Schlögl, Eur. Phys. J. B **28**, 407 (2002).
[51] H. Katzke, P. Tolédano, and W. Depmeier, Phys. Rev. B **68**, 024109 (2003).
[52] T. Tsujioka, T. Mizokawa, J. Okamoto, A. Fujimori, M. Nohara, H. Takagi, K. Yamaura, and M. Takano, Phys. Rev. B **56**, R15509 (1997).
[53] C. B. Stagarescu, X. Su, D. E. Eastman, K. N. Altmann, F. J. Himpsel, and A. Gupta, Phys. Rev. B **61**, R9233 (2000).
[54] F. M. F. de Groot, M. Grioni, J. C. Fuggle, J. Ghijsen, G. A. Sawatzky, and H. Petersen, Phys. Rev. B **40**, 5715 (1989).
[55] J. B. Goodenough, Phys. Rev. **100**, 564 (1955).
[56] J. Kanamori, J. Phys. Chem. Solids **10**, 87 (1959).
[57] J. B. Goodenough, *Magnetism and the Chemical Bond* (Wiley Interscience, New York, 1963).
[58] A. P. Ramirez, Annu. Rev. Mater. Sci. **24**, 453 (1994).
[59] L. Wang, T. Maxisch, and G. Ceder, Phys. Rev. B **73**, 195107 (2006).
[60] K. Momma and F. Izumi, J. Appl. Crystallogr. **44**, 1272 (2011).